# ANALYSIS AND EXPERIMENTAL VERIFICATION OF LOSSES IN A CONCENTRATED WOUND INTERIOR PERMANENT MAGNET MACHINE

## Rukmi Dutta[*], Lester Chong, and Fazlur M. Rahman

University of New South Wales, Australia

**Abstract**—It is well known that additional space harmonics in the air-gap magnetomotive force (MMF) distribution of the concentrated non-overlapping windings (CW) cause additional losses in the machine. This is especially so for machines used for traction applications where the machine requires to operate over its rated speed and frequency. In this paper, the authors investigates losses present in an interior permanent magnet (IPM) machine with CW designed to achieve a very wide field weakening range. Losses were quantified analytically and also using finite element methods. Loss estimations were experimentally verified in a constructed prototype machine. Based on the analysis, key losses were identified. The optimization process to minimize these losses and of improving efficiency were discussed in details. The segregation of the losses in the studied machine indicates that the losses in the magnet are much smaller compared to the rotor and stator core losses caused by the slot harmonics. Therefore, core loss minimization techniques for this type of machine will involve reduction of slot harmonics. Also, copper loss is found to be the most dominating component of the total loss. Hence, copper loss minimization should be part of the design optimization process.

## 1. INTRODUCTION

Concentrated non-overlapping windings (CW) have been steadily gaining popularity for a wide range of applications including washing machines, wind generators, ship propulsion and electric vehicle drives [1]. This is due to a compact design by reduction in end winding length and simplified manufacturing process. The recent work on application of CW in surface permanent magnet synchronous machine

(PMSM) showed its ability to achieve low cogging torque, sinusoidal back electromotive force (EMF) waveforms and very wide constant power speed range (CPSR) [2, 3].

In comparison to surface-type PMSM, interior-type PMSM has robust rotor, additional reluctance torque and rotor saliency which is an added advantage for the sensor-less drive applications.

Authors have studied application of CW in V-shaped interior PM machine for wide CPSR. A full study of various combinations of stator slots and rotor poles was investigated for the CW IPM machine, and the 18-slot, 14-pole combination was chosen due to its intrinsic nature of producing low cogging torque, sinusoidal back electromotive force (EMF) waveforms, larger winding factor and relatively higher saliency ratio. The full design consideration and performance characteristics of this prototype machine were published elsewhere [4]. The aim of this paper is to investigate various losses of the CW-IPM machine and its effect on the field weakening performance.

The magnetomotive force (MMF) waveforms of the concentrated winding stator are rich in harmonic and sub-harmonic contents, consequently leading to an increase in core and magnet losses [5]. However, the presence of these harmonics also causes high slot leakage inductance in the winding; because of which the characteristic current of the PMSM can be made closer to its rated current for achieving wider CPSR [3]. Thus, the application of CW in the PMSM offers wide CPSR and is gaining popularity. The desirable compromise between the CPSR and additional losses in the machine will be worthwhile future study.

The PM machine designed with CW for wide CPSR is most affected by the increase in harmonic related losses due to its nature of operation, of up to several times of the base frequency. Hence, losses and loss minimization techniques for permanent magnet machines with CW have been studied in a number of papers in recent years. Key recent studies include: study of core losses with phase and slot/pole combination variation [6, 7], minimization by variation of rotor core/rotor magnet geometries [8, 9], study of magnet losses [10] and minimization of magnet losses by the use of segmented magnets [11], effects of slot/pole variation [12], effects of winding layers [13, 21].

There are a few papers which studied losses in CW IPM machine [14–16]. These papers present finite element (FE) studies of optimization techniques with specific characteristics. Han et al. in [16] presented a technique to minimize eddy current losses in the stator teeth of IPM rotors under field-weakening conditions. Yamazaki et al. [15] presented a method to reduce magnet eddy current losses at high rotational speeds.

In this paper, authors have used well-established loss minimization techniques for conventional distributed winding (DW) machine to minimize the losses in a CW-IPM machine designed for wide field weakening operation. The aim is to quantify all key losses present in a CW-IPM machine and subsequently verify them experimentally with a constructed prototype. Design concepts will be justified in terms of how losses are minimized. The applied techniques to minimize losses include the application of segmented magnets, variation of magnet type, variation in lamination thickness, as well as different winding methodologies.

## 2. LOSSES IN A CONCENTRATED WINDING PM MACHINE

Compared to DW, the air-gap MMF waveform of the CW contains additional space harmonics and sub-harmonics which do not rotate in sync with the rotor. These additional harmonic components contribute to frequency related losses which occur primarily in the core and magnets of the machine.

Figures 1(a) and 1(b) show magnetic flux distribution of a CW and DW machine of same rotor pole number respectively.

Assuming highly permeable core, no saturation and zero permanent magnet field, the relation between the stator current and the air-gap flux produced by this current can be found as

$$I = \frac{B_s A_{\mathrm{rot}} R_{\mathrm{air}}}{N} \tag{1}$$
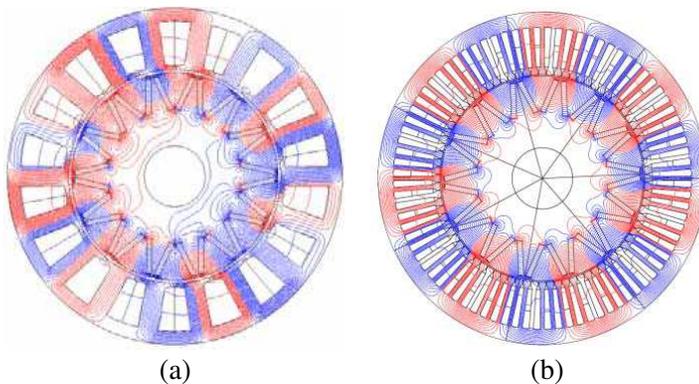


(a)                              (b)

**Figure 1.** 14-pole IPM rotor with (a) fractional-slot CW stator, (b) integral slot DW stator showing magnetic flux distribution.
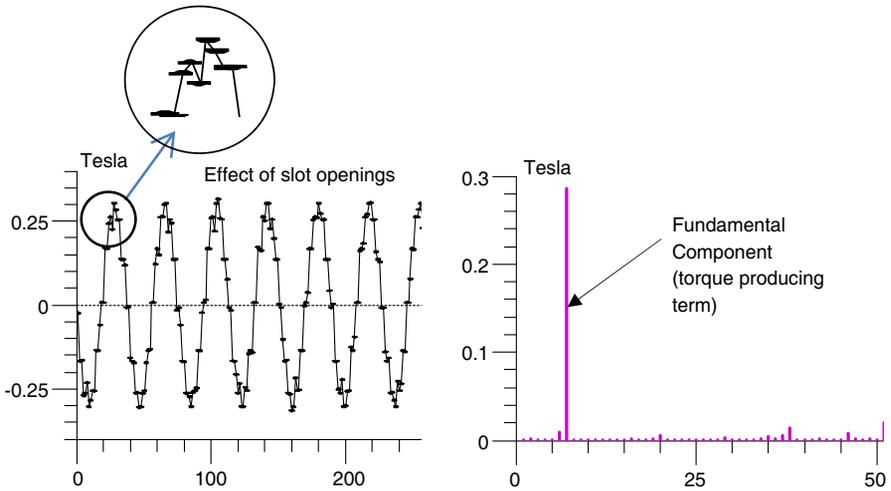
**Figure 2.** Air-gap flux density waveform and harmonic spectrum from the DW stator.

where $B_s$ is the flux density produced by the stator current, $A_{rot}$ the airgap of surface area, $R_{air}$ the air-gap reluctance, and $N$ the number of turns per stator coil.

It is well known that widths of the slot openings contribute to the variation of air gap permeance and cause rotor losses [17]. However, the effect of slot opening is far less in a CW machine compared to effect of MMF space harmonics, specially the slot harmonics. The air-gap flux density waveform produced by the stator current in the DW IPM machine of Figure 1(a) with magnet removed is shown in Figure 2. Figures 3(a) and (b) show the air-gap flux density produced by the stator current for the prototype CW machine of Figure 1(b) with magnet removed.

The close inspection of the flux density waveforms of Figures 2 and 3(a) and (b) reveal that permeance variation due to the slot opening is much small compared to the DW machine. The rotor loss due to these permeance harmonics is therefore, small in a CW machine compared to DW machine. The major part of the rotor loss in CW machine thus is due to the MMF space harmonics.

The harmonic whose order is equal to rotor pole pairs is known as the main or fundamental harmonic which rotates synchronously with the rotor. The harmonics whose orders are lower than the fundamental rotates slower than the rotor and harmonics whose orders are higher than the fundamental rotates faster than the rotor. Among all these harmonics, the ones which have same winding factor as the main or
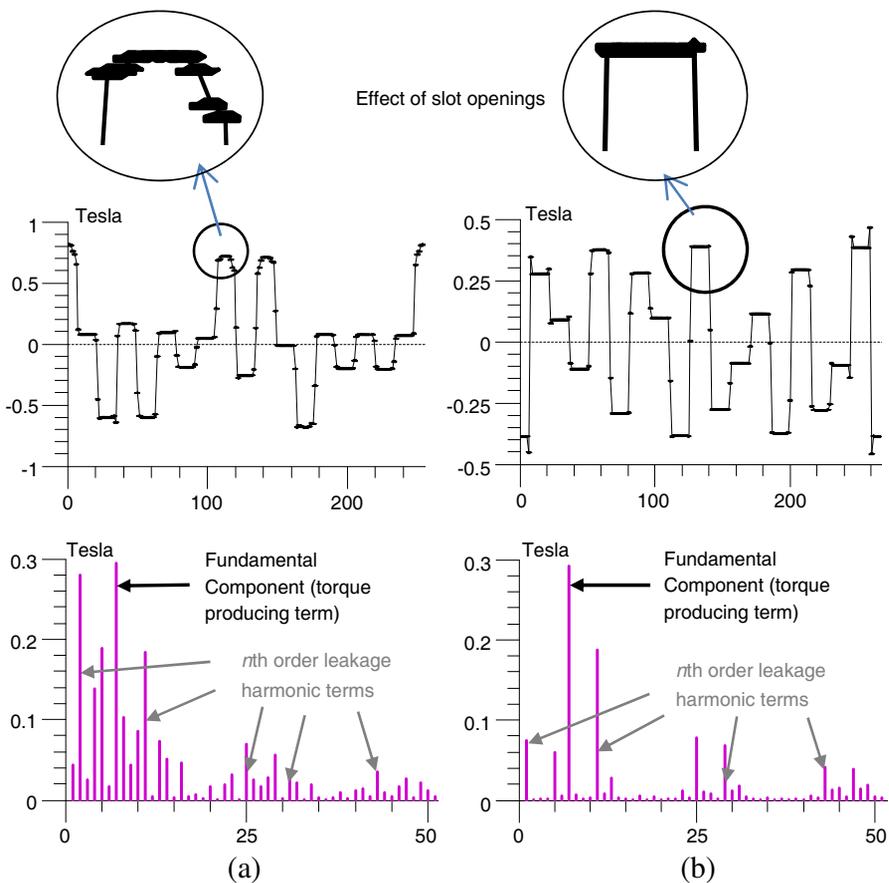
**Figure 3.** Airgap flux density and its frequency spectrum generated by the stator current alone from (a) a single-layer CW stator, (b) a double-layer CW stator.

fundamental harmonic, called slot harmonics contribute most toward the rotor losses [6].

The order of slot harmonic can be found as

$$n_{sh} = kQ \pm p \tag{2}$$

where $k = 0, 1, 2, \ldots, Q$ is slot number and $p$ is pole pairs.

In the prototype 18-slot/14-pole FSCW IPM machine, pole pairs $p$ is 7 and possible slot harmonics are 11, 25, 29 etc.. The machine contains sub harmonics, but not any of them are slot harmonics. Comparing the spectrum of single and double layer CW given in Figures 3(a) and (b) respectively, it can be noticed that slot harmonic

11, 25, 32, . . . are present in both single layer and double layer CW. However, compared to a single layer, double layer has far less over all harmonics. Therefore, a double layer winding was chosen for this study. The asynchronously rotating harmonics cause increased rotor losses. Hence, it is interesting to study rotor losses caused by the slot harmonics.

Total losses in the stator and rotor core are the hysteresis and eddy current loss, which can be expressed generally by (3).

$$P_{\text{core}} = K_e f^2 B_{\max}^2 + K_h f B_{\max}^{\eta_{st}} \tag{3}$$

where,

$K_e$ = Eddy current loss constant,

$K_h$ = Hysteresis loss constant,

$B_{\max}$ = Maximum flux density,

$\eta_{st}$ = Material dependent Steinmetz loss constant (1.6 to 2.0).

Although excess loss can be computed in the FE model using simple statistical data based formula proposed by Berotitti [39], its applicability with PM machine is still under scrutiny. A benchmark study on surface permanent-magnet brushless motor in [40] found a good correlation between experimental and computational data without considering excess losses. Another recent study [41] showed that individual contribution of excess and eddy-current losses cannot be separated. Because of these reasons the excess loss was not considered in this study and hence not included in (3).

While hysteresis loss density depends largely on frequency, material and flux density, the eddy current loss density is proportional to the frequency squared, making it much more susceptible to slot harmonic components, which could be several times higher than the operating frequency. In the field-weakening region, the situation is further exaggerated. For example, during operation at 10 times of the base frequency $50\,\text{Hz}$, a harmonic component at $n = 29$, would corresponds to $14500\,\text{Hz}$.

In order to visualize the proportion of loss densities better, it is common to keep hysteresis term constant and (3) can be simplified [18–20] as

$$\frac{P_{\text{core}}}{f B_{\max}^2} = K_e f + K_h \tag{4}$$

Steinmetz constant was taken as 2 here.

The hysteresis loss is material dependent, and little can be done to minimize it through design variation. Hence, the emphasis will be placed on eddy current loss in which the loss minimization can

be achieved through a number of techniques including well-known technique of selecting lamination thickness. Using Faraday's and Maxwell's equations, the relation between the air-gap harmonics and eddy current loss can be derived (shown in the appendix).

For integral-slot DW, a sinusoidal air-gap flux density shown in the Figure 2 can be assumed, eddy current loss is given as:

$$P_{\text{eddy}} = \frac{\tau^2 \sigma}{12} \left( \frac{dB}{dt} \right)^2 = \left[ \frac{\tau^2 \sigma}{6} \left( 1 + \cos 2\omega t \right) \right] f^2 B_{\max}^2 \qquad (5)$$

where the terms in the square brackets are usually termed as the eddy current loss constant.

In CW, the function would not only depend on the fundamental but other significant harmonic components, specially the slot harmonics. Eddy current loss for CW can thus be generally expressed as (6), where $B_n$ is the magnitude of the $n$th harmonic component of the waveform shown in Figures 3(a) and (b).

$$P_{\text{eddy}} = \frac{\tau^2 \sigma}{12} \left( \frac{d}{dt} B_n \sum_{n=1}^{N} \frac{1}{n} \sin \left( n\omega t \right) \right)^2 \qquad (6)$$

The inclusion of additional harmonic components is unavoidable with CW; however, compared to single-layer, the double-layer CW has less harmonic terms as shown in Figure 3(b). It was confirmed in [2] that a higher layer number increases efficiency by eliminating eddy current losses of some harmonic terms. Therefore, double-layer CW was preferable and selected for this work. However, it should be noted here that double layer winding does not eliminate the slot harmonics as shown in Figure 3(b).

# 3. STUDY AND QUANTIFICATION OF LOSSES IN THE PROTOTYPE MACHINE

The electrical losses of a PM AC machine include, i.e., eddy current and hysteresis losses in the stator and rotor cores, eddy current and hysteresis loss in the permanent magnet and copper loss of the stator winding. The mechanical losses include mostly bearing/friction losses and windage losses.

## 3.1. Core Losses

As shown in (3), core losses consist of hysteresis and eddy current losses. One method of separating these two losses is derived in [22]. According to this derivation, in typical steel laminations, hysteresis loss
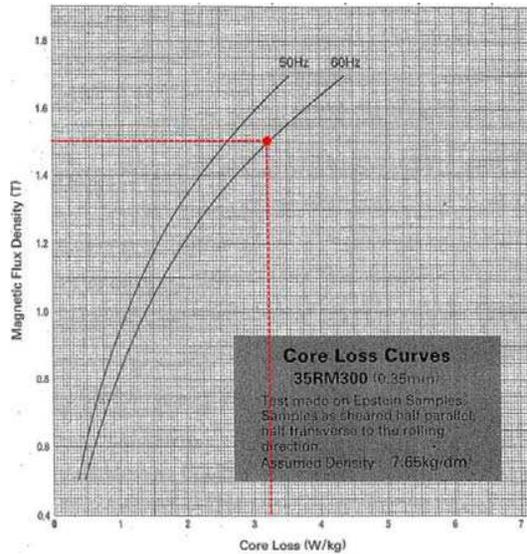
**Figure 4.** Core loss curve of 35RM300 provided by *Sankey* showing core loss at 60 Hz/1.5 T.

at 60 Hz make up approximately 67% of the total core loss while the rest of the losses comprise of eddy current and other types of losses.

The core material used in the prototype CW IPM machine is 35RM300. The loss density curve provided by the material manufacturer is shown in Figure 4 and using the relation derived in [20], the estimated loss densities of the used laminated material are found to be 1.08 W/kg for eddy current loss and 2.17 W/kg for hysteresis loss at 60 Hz and 1.5 T.

In order to determine the core losses due to harmonic components for various operating frequencies, the eddy current and hysteresis loss constants (K_e and K_h) must first be found for the selected laminated steel.

A narrow annular-core specimen consisting of thin laminations was modeled to find the loss constants K_e and K_h of 35RM300 from a FE model which are 0.29 and 151 respectively. These loss constants were used to obtain the core loss at various excitation frequencies in the FE model of the CW IPM machine. The FE package used in this paper is Flux 2D/3D from Magsoft/Cedrate.

The calculated hysteresis and eddy current loss constants, and some other key features for the three laminated steel grades examined are shown in Table 1. The calculated losses from the FE model at 50

**Table 1.** Key features of three core material types.

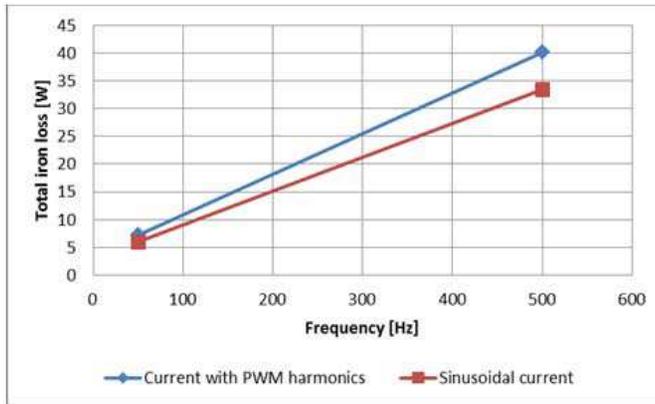|  | 35RM300 | 50JN350 | 65JN800 |
|---|---|---|---|
| **Lamination thickness** | 0.35 mm | 0.50 mm | 0.65 mm |
| **Sat. mag. ($B_{50}$)** | 1.68 T | 1.68 T | 1.72 T |
| **Stacking factor** | 95% | 96% | 97% |
| **Total core loss (@60 Hz/1.5 T)** | 3.25 W/kg | 4.45 W/kg | 10.15 W/kg |
| **$K_h$** | 151 | 263 | 495 |
| **$K_e$** | 0.29 | 0.39 | 0.89 |



**Figure 5.** Calculated iron loss in FE model with and without PWM harmonics in the current.

and 500 Hz for all three grades are shown in Figure 6.

It should be noted here that, the inverter used in the experimental set-up uses 10 kHz carrier frequency. Figure 5 below compares calculated core loss for 50 Hz and 500 Hz in the FE model with sinusoidal current and current with PWM harmonics. The calculated core loss of PWM inverter-fed machine is about 1.2 times higher. Since this increase of loss due to the PWM harmonics in the current is relatively insignificant, the input currents were considered as pure sinusoid for subsequent FE calculations.

It can be observed in Figure 6 that both stator and rotor core losses in the constant torque region (50 Hz) is low (< 2.5% of output power). However, in the higher field-weakening region (500 Hz), the core loss becomes significant (> 13% of the output power). This would result in almost a 10% difference in efficiency.

The results emphasize the importance of using thin laminations with low losses when designing machines for field-weakening
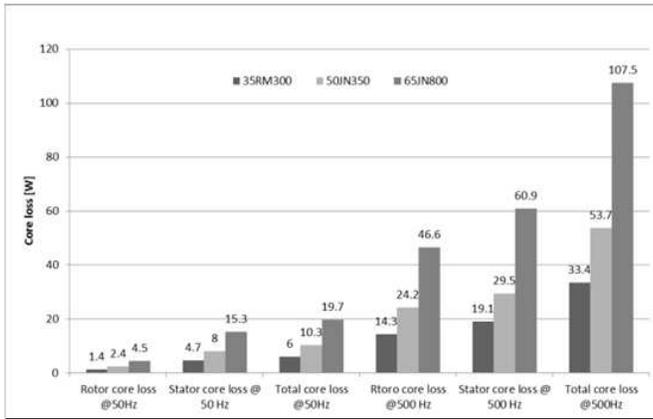
**Figure 6.** Core loss comparison at 50 and 500 Hz with different steel grades.
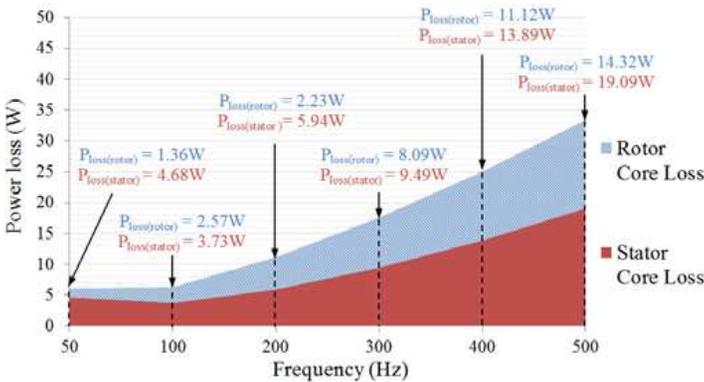


**Figure 7.** Core loss with chosen steel grade at various frequencies.

applications. Thicker laminations like the 65JN800 are more suitable for machines operating at lower frequencies or with constant torque where torque density is of higher priority. Thus, the chosen steel grade for the prototype design is 35RM300. The breakdown of losses at various frequencies obtained from the FE model is shown in Figure 7.

As expected, core loss increases with frequency. The percentage of stator to rotor core loss is several times higher in the low frequency or constant torque region. In the field-weakening or high frequency region, rotor core losses also become substantial; contributing to a large part of the total core loss in the machine. As explained in Section 2, rotor core losses, especially the eddy current loss is contributed mostly by the
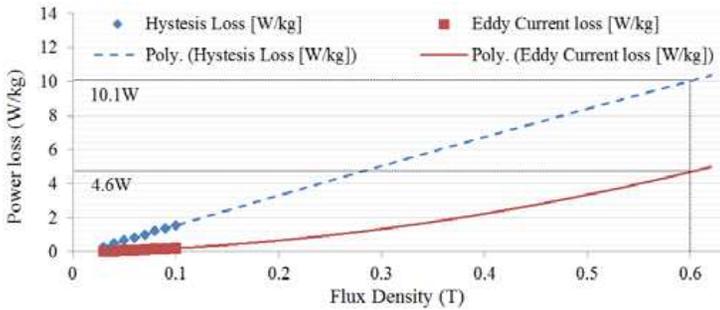
**Figure 8.** Extrapolated values of measured hysteresis and eddy current loss for sintered neodymium magnets at 50 Hz from [1, 2].

air-gap slot harmonics. Reduction of these harmonics would make a significant difference to the efficiency. Thus, one of the future research challenges of CW-PM machine is the development of techniques to reduce these harmonics.

## 3.2. Magnet Losses

It is well-known that the time varying magnetic fields may create substantial losses in the magnets, (especially in SPM machines). A great deal of research interest is focused on the study and minimization of magnet losses in CW permanent magnet machines. Commonly used strategies to reduce magnet losses are by the use of bonded instead of sintered magnets, at the expense of lower magnet strength, or the use of sintered-segmented magnets [23–27].

It was explained in [24] that, in a polarized magnet, losses are much smaller than those of the non-polarized one. While there has been a significant amount of study on eddy current losses in magnets of PM synchronous machines, an in-depth study on hysteresis loss is not available. The phenomenon of hysteresis in a polarized and non-polarized NdFeB magnet was studied in [28]. It appears that hysteresis can happen in a polarized magnet if minor loops form due to load and temperature variation. According to [10], hysteresis losses in a polarized magnet can be significant specially, when slot harmonics in the machine is high. The FSCW IPM machine falls in the category of machines with high slot harmonics. In order to ensure that hysteresis loss of the magnet is not particularly of concern in the prototype FSCW IPM machine, a study of this loss was also conducted. The NdFeB used in the prototype is N24EH from Raremag® with remanence of 1.04 T.

In [10, 24, 29] hysteresis losses in synchronous machines were

studied based on a combination of measurements and FE results. In this paper hysteresis loss of the CW-IPM machine was estimated using experimental data provided in [10, 24, 29]. The magnet losses were measured from 30 to 150 Hz and 0.01 to 0.1 T using a closed-type measuring equipment. The measured losses were separated to eddy current loss and hysteresis loss by two-frequency method. The measured losses were plotted against flux density. Since the losses were measured only up to 0.1 T, the extrapolated polynomial trend-lines were fitted into measured data of [10, 24] to estimate the hysteresis loss of the magnet in the prototype CW-IPM machine which is shown in Figure 8. For this work, this estimation would suffice as it will be shown later that magnet losses in the CW-IPM machine make up a very small percentage (0.5%) of the total losses.

The typical operating point of the permanent magnets in the prototype CWIPM machine is 0.6 T. Loss density values obtained from the extrapolation at this flux density are 10.1 W/kg for hysteresis and 4.6 W/kg for eddy current loss, (at 50 Hz) as show in Figure 8.

For the neodymium magnets, conductivity is readily available from the data sheets. Thus, the eddy current loss constant can be calculated from the following formula

$$K_e = \sigma \frac{\tau^2 \pi^2}{6} \tag{7}$$

With each magnet piece being 79 mm long, K_e for sintered and bonded neodymium magnets are calculated to be 6416 and 73 respectively. These values were used in a 3D finite element model, (shown in Figure 9), to calculate magnet eddy current loss. Sintered magnets were chosen over bonded magnets due to its higher remnant
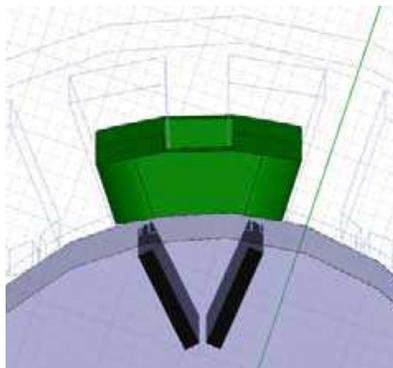


**Figure 9.** 3D model of a single pole and single phase excitation with V-shaped IPM.

flux densities and operating temperatures. The breakdown of losses at various frequencies for the sintered magnets, obtained from the FE model, is shown in Figure 10.

The CW surface permanent magnet (SPM) machines have permanent magnets that are directly exposed to air gap flux harmonics. Thus, higher magnet losses are expected in such machine [30]. Bonded NdFeB has been used in such machines to reduce magnet losses. In CW-IPM machine, magnets are buried in the rotor iron, hence they
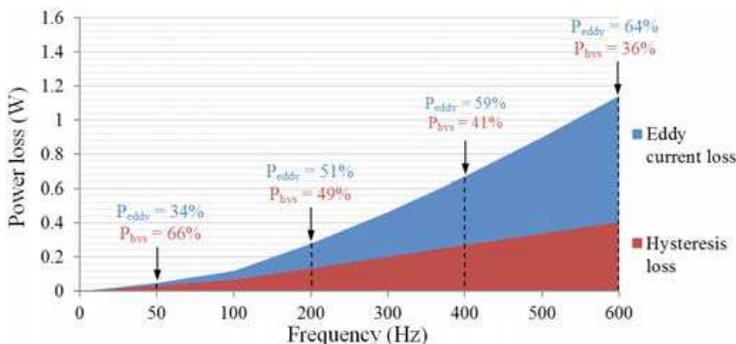


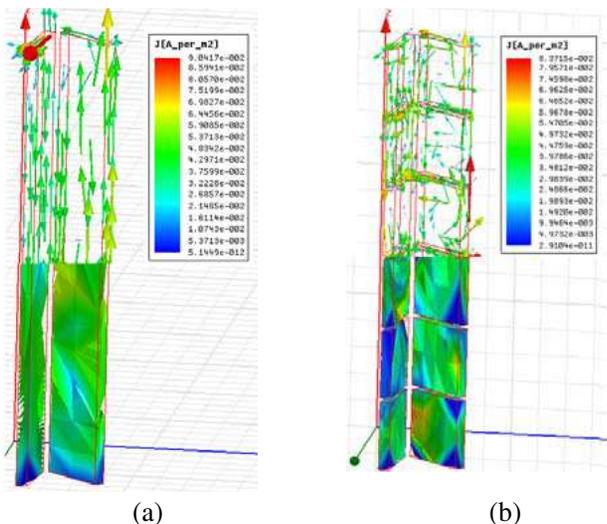**Figure 10.** Breakdown of losses in sintered NdFeB magnets.



**Figure 11.** Circulating eddy currents in (a) non-segmented poles and (b) segmented poles IPM machine.
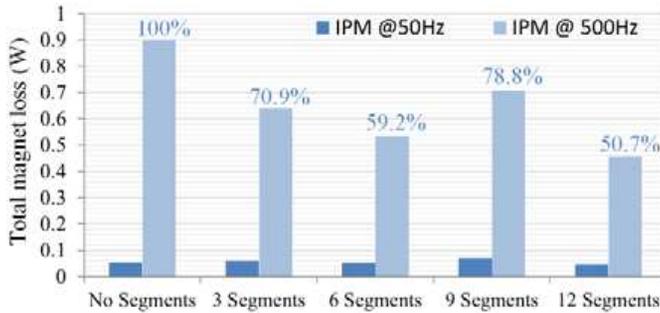
**Figure 12.** Magnet losses with various magnet segments.

are less exposed to the MMF harmonics. Consequently, magnet loss in this type of machine is much less compared to a CW-SPM machine. Therefore, there is no justification of using bonded magnet in this type machine for the sole purpose of reducing magnet losses.

There are different techniques to reduce magnet loss in the CW-SPM machine which uses sintered NdFeB. One of such techniques is segmentation of the magnet piece in the axial direction. Epoxy magnet coating serves as the insulation between each layer. The effects of segmenting sintered neodymium magnets have been thoroughly studied — key work in this area includes [23, 25, 31–33]. In [33] work done by Yamazaki et al., magnet losses in different rotor types due to carrier and slot harmonics where compared. With the increased number of segments, a gradual decrease of the magnet eddy current losses can be observed in a SPM machine whereas in an IPM machine, the decrease is not gradual.

In this work, the effect of segmenting V-shaped IPM is also investigated. Figure 11(a) shows the circulating eddy currents in the non-segmented pieces of the V-shaped pole magnet, (b) shows the same in the segmented pieces. These results were obtained from the 3D FE model of the CW-IPM machine.

The total magnet losses obtained at 50 and 500 Hz for the CW-IPM machine was shown in Figure 12.

It can be observed from the Figure 12 that the magnet loss initially reduces with increased number of segments but then peaks with 9 segments; thus, complying with Yamazaki's findings in [11, 33]. With 12 segments, the loss has reduced by about 50%. However, since the total magnet loss is insignificant making up for a mere 0.5% of the total loss, it is arguable whether magnet segmentation is necessary in a CW-IPM machine.

### 3.3. Stator Winding Copper Losses

Stator winding loss — also known as $I^2R$, copper or joule loss,is generated when the armature windings are excited by an external source. Of the total loss in PM machines, the largest portion is usually due to $I^2R$ loss [34]. If the chosen copper conductors are sufficiently thin, the skin effect is negligible and hence, $I^2R$ can reasonably assume to be frequency independent.

$I^2R$ loss is described in the following formula:

$$I^2R = 2N_{\text{coil}}I^2\rho\frac{l_{eff}}{A_w} \qquad (8)$$

where,

$N_{\text{coil}}$ = Number of turns per coil,

$\rho$ = Conductor resistivity ($1.68 \times 10^{-8}$ for copper),

$A_w$ = Cross-sectional area of wire.

The slot area in the stator can be maximized by optimizing tooth and yoke area so that the flux densities in these areas are kept just under the saturating limit of the core. With a fixed slot area, the only way to increase conductor size and lower $I^2R$ loss is by increasing the slot-fill factor ($S_{ff}$) given by the following equation:

$$S_{ff} = \frac{N_{\text{coil}}A_w}{A_s} \qquad (9)$$

Typical slot-fill factors achievable by commercial winders are in the range of 35% to 44%. Approximately 60% can be achieved by highly skilled winders [35, 36]. Unlike DW, which overlap one or more stator teeth, CW are wound around individual stator teeth. The coil around individual stator teeth can take advantage of more advanced winding methods, such as the joint lapped core methods [35, 37] and use of modular stator tooth pieces [36]. These methods claimed to achieve up to 75% and 78% slot-fill factor respectively.

Concentrated windings can be wound in one of two methods: the horizontal slot-fill method, as shown in Figure 13(a), or the vertical slot-fill method, as shown in 13(b). The prototype machine is wound using the former method to keep the winding process simple and cheaper.

The prototype machine has 115 turns per coil, and 6 coils per phase. The slot-fill factor achieved with American wire gauge (AWG) 22 was 41%. The measured length of 1 turn is 276 mm as shown in Figure 13(a). Due to the high number of turns used, winding resistance per phase amounted to 10 Ω. The rated current of the machine is 2.2 A/ph. Thus, total copper loss under full load operating condition
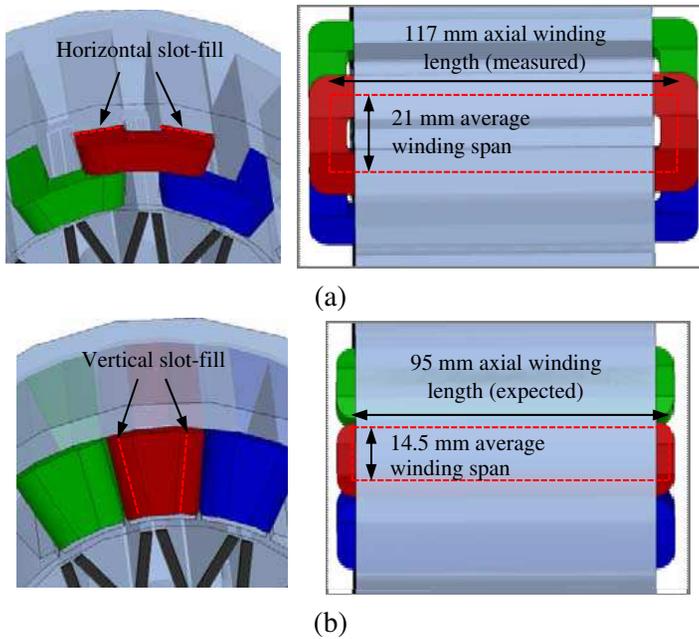
**Figure 13.** Slot-fill methods, (a) horizontal slot-fill method, (b) vertical slot fill winding method.

is about 145 W (18% of the total output power). As it can be seen from the measured loss break-down given in Table 3, it is the most significant loss of the prototype machine.

## 4. MECHANICAL LOSSES

Mechanical losses consist of mainly bearing and windage losses [18, 34, 38]. Bearing loss is dependent on factors such as the bearing type, bearing diameter, rotor speed, load and lubricant used. Windage loss occurs when friction is created with the rotating parts of the machine and the surrounding air.

Bearing losses can be calculated with the following formula:

$$P_{\text{bearing}} = 0.5\omega_m k_b F D_b \tag{10}$$

where,

$\omega_m$ = Mechanical speed of the rotor,

$k_b$ = Bearing loss constant,

$F$ = Force acting on the bearing,

**Bearing 1**
Inner diameter = 20 mm
Bearing constant = 0.0015

**Bearing 2**
Inner diameter = 17 mm
Bearing constant = 0.0015

**Rotor core**
Density = 7650 kg/m³
Total Mass = 2.182 kg

**Magnets**
Density = 7500 kg/m³
Total Mass = 0.448 kg

**Shaft**
Density = 8000 kg/m³
Total/Mass = 0.650 kg

**End plants**
Density = 8000 kg/m³
Total Mass = 0.30 kg
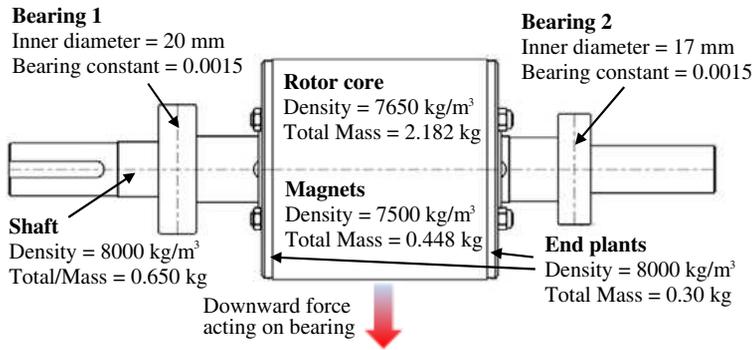
Downward force
acting on bearing

**Figure 14.** Key components contributing to the weight of the rotor.

$D_b$ = Bearing inner diameter.

The Figure 14 shows the drawing of the IPM rotor highlighting the mechanical parts responsible for losses. The mass is calculated based on the known volume and density of the various materials used. Bearing friction loss occurs in both bearings. From the estimated weight of the rotor, the downward force acting on the bearings can be calculated from

$$F = mg \qquad (11)$$

where,

$m$ = Mass of the rotor,

$g$ = Gravity $(9.81 \, \text{m/s}^2)$.

Unlike frictional loss,windage loss increases non-linearly with speed. The rotor can be modeled as a rotating cylinder in an enclosure and power loss can be modeled as the resisting drag torque on the cylinder. This can be expressed as follows [3]:

$$P_{\text{windage}} = 0.03125\omega_m^3 \pi k_{ct} k_r \rho_{\text{air}} D_r^4 l_r \qquad (12)$$

where,

$k_{ct}$ = Torque coefficient (which has to be separately determined),

$k_r$ = Roughness coefficient (between 1–1.4),

$\rho_{\text{air}}$ = Density of air $(1.184 \, \text{kg/m}^3)$,

$D_r$ = rotor diameter,

$l_r$ = rotor length.

To determine the torque coefficient, the Couette Reynolds number needs to be determined first. The Reynolds number $N_{Re}$ is given as:

$$N_{Re} = \frac{\rho_{\text{air}}\omega_m D_r l_{ag}}{2\mu_{\text{vis(air)}}} \tag{13}$$

where,

$l_{ag}$ = Airgap length,

$\mu_{\text{vis(air)}}$ = Dynamic viscosity of air $(18.6\,\mu\text{Pa})$.

For $N_{Re}$ between 64 and 500, the torque coefficient is given as,

$$k_{ct} = 2\frac{(2l_{ag}/D_r)^{0.3}}{(N_{Re})^{0.6}} \tag{14}$$
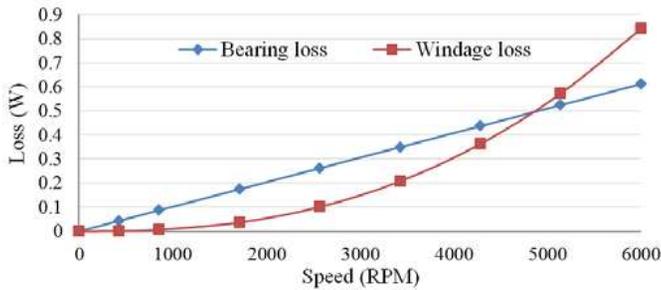


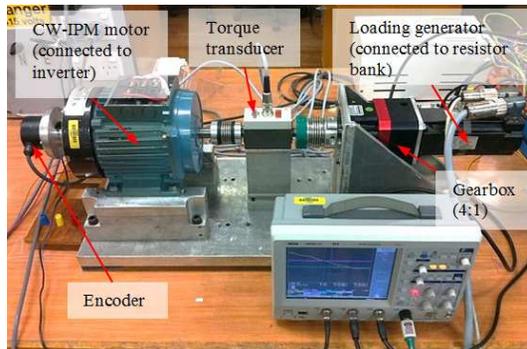**Figure 15.** Calculated bearing and windage losses for the prototype machine.



**Figure 16.** Experimental setup to measure losses and field-weakening performance of the prototype machine.

And for $N_{Re}$ between 500 and 50000, the torque coefficient is given by:

$$k_{ct} = 1.03 \frac{(2l_{ag}/D_r)^{0.3}}{(N_{Re})^{0.5}} \tag{15}$$

Using (10) and (12), windage and friction losses of the prototype machine are calculated for various speeds are shown in Figure 15.

## 5. EXPERIMENTAL VERIFICATION OF TOTAL LOSS

Figure 16 shows the experimental set-up used to measure the performance of the constructed prototype machine. Table 2 shows some key parameters of the machine.

Table 3 shows the segregation of the measured losses: copper, core, magnet, bearing and windage loss. No load losses at various speeds were measured with and without the magnet inserted in the rotor. Thus, core loss and magnet losses were segregated. By driving the prototype machine without the magnet excitation by another machine with known losses, total mechanical losses were measured. Windage and friction losses were segregated from the total mechanical loss after calculating the windage loss using Equation (12). Copper loss was calculated using measured resistance and current.

**Table 2.** Key specifications of the 800 W CW-IPM machine.

| | |
|---|---|
| Stator outer diameter | 130 mm |
| Rotor outer diameter | 80 mm |
| Air-gap length | 1.2 mm |
| Stack length (stator) | 80 mm |
| Stack Length (rotor) | 79 mm |
| Number of poles | 14 poles |
| Number of slots | 18 slots/double-layer |
| Rated voltage | 320 V$_{rms}$/phase |
| Rated current | 2.2 A$_{rms}$/phase |
| Magnet remnant flux density | 1.04 T |
| Core material | Non-oriented FeSi |
| Saturation mag. of laminations | 1.68 T@5000 A/m |
| Predicted core loss at 50 Hz/1.5 T | 2.60 W/Kg |
| Slot-fill factor | 41% |
| Copper loss | 10 Ω/ph |

**Table 3.** Loss breakdown of the 800 W CW-IPM machine.

| Freq. | Copper Loss | Core Loss | Magnet Loss | Friction Loss | Windage Loss |
|-------|-------------|-----------|-------------|---------------|--------------|
| 50    | 142.5       | 6.04      | 0.052       | 0.044         | 0.001        |
| 100   | 142.5       | 6.3       | 0.120       | 0.087         | 0.007        |
| 200   | 142.5       | 11.17     | 0.280       | 0.175         | 0.037        |
| 300   | 142.5       | 17.58     | 0.465       | 0.262         | 0.101        |
| 400   | 142.5       | 25.01     | 0.673       | 0.35          | 0.208        |
| 500   | 142.5       | 33.41     | 0.900       | 0.437         | 0.363        |
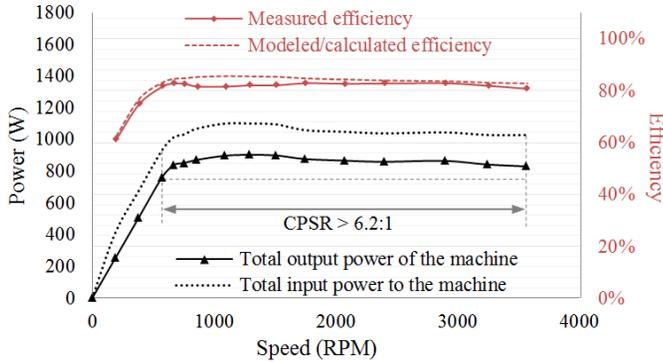


**Figure 17.** Verification of measured efficiency throughout a 6.2 : 1 field-weakening range.

It can be seen from this Table 3 that the largest percentage of losses arise from copper loss, which makes up 84.8% of the total loss at maximum speed, followed by the core loss which makes up 14.6%. Compared to these two losses, the other losses are extremely small.

Figure 17 compares output, input powers and efficiency obtained from the FE model with the measured values from the experimental setup. The field-weakening performance indicating the constant power speed range (CPSR) is also shown in the same figure.

## 6. EFFICIENCY OPTIMIZATION STUDY

The results in the previous section show that the majority of losses in the prototype machine arise from the copper loss. It should be noted here that the design of the prototype machine was optimized with a
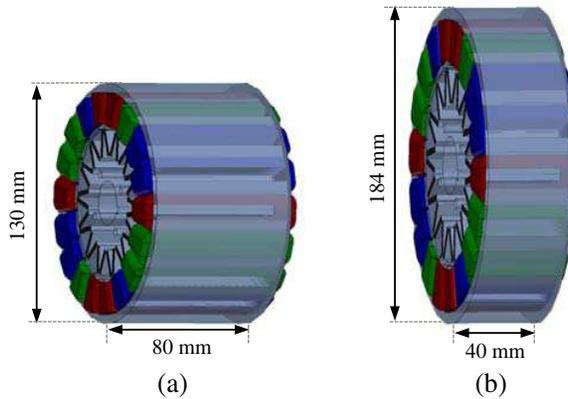
**Figure 18.** Two different optimized designs, (a) IPM-Eq and (b) IPM-Short.

size constraint. This 800-W CW-IPM machine was designed to fit into the frame size of a commonly used 4-pole, 550 W induction machine. Because of this size constraint, there was not enough room to increase slot area to create space for larger conductor size to reduce copper losses.

An efficiency optimization study of the prototype machine was carried out by removing the size constraint.

Figure 18 shows two possible methods in which the slot size can be increased by: i) keeping the stator outer diameter and stack length same as the constructed prototype, but reduce the stator inner diameter allowing a reduced volume for the rotor to make space for a larger stator width; (ii) decreasing the stack length to half while increasing the stator outer diameter proportionally. The total machine volumes in the both designs are kept same as the constructed prototype machine for a fair comparison. For convenience sake, these two designs will be called IPM-Eq (for the design with equal dimensions, but reduced rotor size) and the IPM-Short (for the design with reduced stack length).

Key parameters for the two designs are shown in Table 4. To ensure designs are practical, the slot-fill factor is set at 45%.

Figures 19(a) and 19(b) give the performance characteristics for CW IPM-Eq and CW IPM-Short respectively obtained from the FE models.

It can be seen in Figures 19(a) and (b) efficiencies of the IPM-Eq is over 91% and IPM-Short is over 93% in the whole operating speed range. Both models produce between 900 W to 1 kW of power over a

**Table 4.** Key specifications of the two optimized CW-IPM machine designs.

|  | IPM-Eq | IPM-Short |
|---|---|---|
| Total machine volume | $1.06e^{-3}\,\mathrm{mm}^3$ | $1.06e^{-3}\,\mathrm{mm}^3$ |
| Stator outer diameter | 130 mm | 183.85 mm |
| Rotor outer diameter | 36 mm | 45.7 |
| Slot opening width | 1.2 mm | 1.2 mm |
| Stack length | 80 mm | 40 mm |
| Rated current | $2.2\,\mathrm{A_{rms}/ph}$ | $2.2\,\mathrm{A_{rms}/ph}$ |
| Conductor size | AWG 20 | AWG 21 |
| No. of turns per coil | 163 turns | 127 turns |
| Stator resistance | $4.5\,\Omega/\mathrm{ph}$ | $5.5\,\Omega/\mathrm{ph}$ |
| Mag. remanent flux | 1.13 T | 1.13 T |
| Slot-fill factor | 45% | 45% |
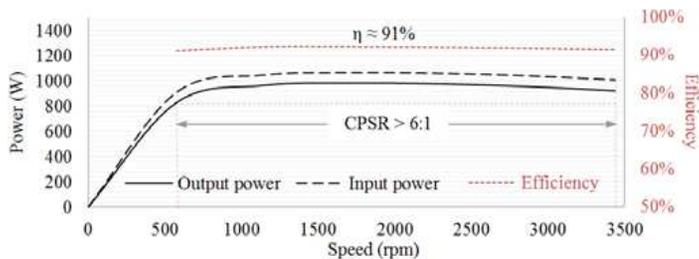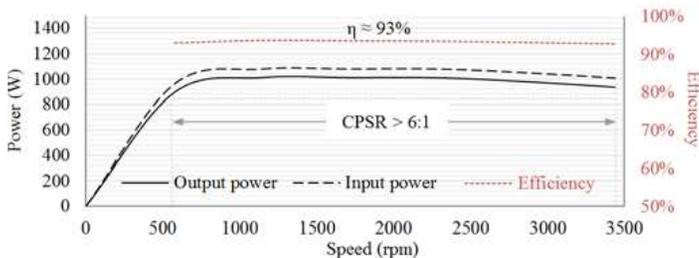


**Figure 19.** Simulated efficiency and power versus speed performance. (a) IPM-Eq, (b) IPM-Short.

6 : 1 CPSR. Between the two models, the IPM-Short resulted in higher efficiency despite higher copper loss. This was due to its capability of producing higher power density (with peak power slightly over 1 kW) as compared to the IPM-Eq.

## 7. CONCLUSION

This paper investigated losses in the CW-IPM machine designed for wide field-weakening applications. This study has revealed a few intriguing facts about losses in a CW-IPM machine:

(i) In CW-IPM machine losses of the magnet is not a significant concern as it is in a CW-SPM machine. Magnet loss minimization techniques may not be as important.

(ii) Various techniques to reduce rotor and stator core loss are very important. The rotor loss is mainly caused by the asynchronously rotating slot harmonics. One of the future design challenges for the CW-IPM machine is to develop techniques to reduce these slot harmonics.

(iii) Copper loss minimization is also very important for high efficiency. Careful consideration of the slot-area during the design optimization process can lead to minimization of copper loss significantly.

Thus, for a CW-IPM machine, rotor and stator core loss and copper loss are the main concern. Well-established techniques such as use of thin lamination sheet are still the best core loss minimization technique for such machine. The presence of asynchronously rotating slot harmonics which cause additional rotor losses depends on slot number and pole pairs. Careful selection of slot and pole number can eliminate some of these harmonics. For example when slot number is equal or higher than the pole number, sub-slot harmonics will be eliminated.

Copper loss minimization can be linked to maximization of slot area for a given dimension. Use of modular stator design can further reduce end-winding length of a FSCW which can also reduce copper loss by reducing winding effective length for a given dimension.

Authors hope that this detailed study of the loss analysis will help future designers of the CW IPM machines to make appropriate design decisions.

## APPENDIX A.

Equating the electric field ($\bar{E}$) in a closed path $c$ along the surface to the induced voltage ($v_{\mathrm{ind}}$) and flux linkage ($\lambda$):

$$\oint_c \bar{E} \cdot dl = v_{\text{ind}} = \frac{d}{dt} \int_s \bar{B} \cdot ds = \frac{d\lambda}{dt} \tag{A1}$$

The current density $J$ and the electric field is related by the conductivity $\sigma$,

$$J = \sigma E \tag{A2}$$

If a fluctuating magnetic flux density $(B)$ acts on a thin piece of material with conductivity $(\sigma)$, thickness $(\tau)$ and width $(w)$. Eddy current $(P_{\text{eddy}})$ induced in this conductor can be expressed as follows:

$$P_{\text{eddy}} = \frac{1}{\tau w} \int \frac{J^2}{\sigma} dv \tag{A3}$$

Assuming that flux density is uniform across the surface, flux linkage will be:

$$\lambda = B\tau w \tag{A4}$$

The induced voltage can be expressed as:

$$v_{\text{ind}} = \frac{d\lambda}{dt} = \tau w \frac{dB}{dt} \tag{A5}$$

If $\tau$ is reduced to infinitely thin sections $(x)$, the electric field along the closed path in can be described by:

$$E = \frac{v_{\text{ind}}}{2w} = x \frac{dB}{dt} \tag{A6}$$

From (A2) and (A6), the induced current density at the surface of the material is given by:

$$J = \sigma E = \sigma x \frac{dB}{dt} \tag{A7}$$

The Eddy current loss shown in (A3) in terms of the induced current density can be described as follows:

$$P_{\text{eddy}} = \frac{1}{\tau w} \int_{-\tau/2}^{\tau/2} \frac{1}{\sigma} \left( \sigma x \frac{dB}{dt} \right)^2 w dx \tag{A8}$$

$$P_{\text{eddy}} = \frac{\tau^2 \sigma}{12} \left( \frac{dB}{dt} \right)^2 \tag{A9}$$

## REFERENCES

1. El-Refaie, A. M., "Fractional-slot concentrated-windings synchronous permanent magnet machines: Opportunities and challenges," *IEEE Transactions on Industrial Electronics*, Vol. 57, 107–121, 2010.

2. Cros, J. and P. Viarouge, "Synthesis of high performance PM motors with concentrated windings," *IEEE Transactions on Energy Conversion*, Vol. 17, 248–253, 2002.

3. El-Refaie, A. M. and T. M. Jahns, "Optimal flux weakening in surface PM machines using fractional-slot concentrated windings," *IEEE Transactions on Industry Applications*, Vol. 41, 790–800, 2005.

4. Chong, L., "Design of an interior permanent magnet machine with concentrated windings for field weakening applications," Ph.D. Thesis, School of Electrical Engineering and Telecommunications, The University of New South Wales, 2012.

5. Bottauscio, O., G. Pellegrino, P. Guglielmi, M. Chiampi, and A. Vagati, "Rotor loss estimation in permanent magnet machines with concentrated windings," *IEEE Transactions on Magnetics*, Vol. 41, 3913–3915, 2005.

6. Fornasiero, E., N. Bianchi, and S. Bolognani, "Slot harmonic impact on rotor losses in fractional-slot permanent-magnet machines," *IEEE Transactions on Industrial Electronics*, Vol. 59, 2557–2564, 2012.

7. Seo, J.-H., S.-Y. Kwak, S.-Y. Jung, C.-G. Lee, T.-K. Chung, and H.-K. Jung, "A research on iron loss of IPMSM with a fractional number of slot per pole," *IEEE Transactions on Magnetics*, Vol. 45, 1824–1827, 2009.

8. Yamazaki, K. and H. Ishigami, "Rotor-shape optimization of interior-permanent-magnet motors to reduce harmonic iron losses," *IEEE Transactions on Industrial Electronics*, Vol. 57, 61–69, 2010.

9. Han, S.-H., T. M. Jahns, W. L. Soong, M. K. Guven, and M. S. Illindala, "Torque ripple reduction in interior permanent magnet synchronous machines using stators with odd number of slots per pole pair," *IEEE Transactions on Energy Conversion*, Vol. 25, 118–127.

10. Fukuma, A., S. Kanazawa, D. Miyagi, and N. Takahashi, "Investigation of AC loss of permanent magnet of SPM motor considering hysteresis and eddy-current losses," *IEEE Transactions on Magnetics*, Vol. 41, 1964–1967, 2005.

11. Yamazaki, K. and Y. Fukushima, "Effect of eddy-current loss reduction by magnet segmentation in synchronous motors with concentrated windings," *IEEE Transactions on Industry Applications*, Vol. 47, 779–788, 2011.

12. Ishak, D., Z. Q. Zhu, and D. Howe, "Comparison of PM brushless motors, having either all teeth or alternate teeth wound," *IEEE*

*Transactions on Energy Conversion*, Vol. 21, 95–103, 2006.

13. El-Refaie, A. M. and T. M. Jahns, "Impact of winding layer number and magnet type on synchronous surface PM machines designed for wide constant-power speed range operation," *IEEE Transactions on Energy Conversion*, Vol. 23, 53–60, 2008.

14. Chong, L., R. Dutta, and M. F. Rahman, "Application of concentrated windings in interior permanent magnet machine," *Australasian Universities Power Engineering Conference, 2007, AUPEC 2007*, 1–5, 2007.

15. Yamazaki, K., Y. Kanou, Y. Fukushima, S. Ohki, A. Nezu, T. Ikemi, and R. Mizokami, "Reduction of magnet eddy-current loss in interior permanent-magnet motors with concentrated windings," *IEEE Transactions on Industry Applications*, Vol. 46, 2434–2441, 2010.

16. Seok-Hee, H., T. M. Jahns, and Z. Q. Zhu, "Analysis of rotor core eddy-current losses in interior permanent-magnet synchronous machines," *IEEE Transactions on Industry Applications*, Vol. 46, 196–205, 2010.

17. Alberti, L., E. Fornasiero, N. Bianchi, and S. Bolognani, "Impact of rotor losses in a 12-slot 10-pole axial flux PM machine," *IEEE Industry Applications Society Annual Meeting, 2008, IAS'08*, 1–8, 2008.

18. Advaced MotorTech, LLC, "Short course on the design of interior permanent magnet and brushless DC machines — Taking theory to practice," May 2010.

19. CEDRAT, *Flux 9.30 User Guide Vol. 3: Physical Applications (Magnetic, Electric, Thermal)*, Apr. 2006.

20. Goldman, A., *Modern Ferrite Technology*, 2nd Edition, Springer, 2006.

21. Reddy, P. B., A. M. El-Refaie, and H. Kum-Kang, "Effect of number of layers on performance of fractional-slot concentrated-windings interior permanent magnet machines," *2011 IEEE 8th International Conference on Power Electronics and ECCE Asia (ICPE & ECCE)*, 1921–1928, 2011.

22. Yeadon, W. H. and A. W. Yeadon, *Handbook of Small Electric Motors*, McGraw-Hill, 2001.

23. Jussila, H., P. Salminen, A. Parviainen, J. Nerg, and J. Pyrhonen, "Concentrated winding axial flux permanent magnet motor with plastic bonded magnets and sintered segmented magnets," *18th International Conference on Electrical Machines, ICEM*, 1–5, 2008.

24.  Shinichi, K., T. Norio, and K. Takeharu, "Measurement and analysis of AC loss of NdFeB sintered magnet," *Electrical Engineering*, Vol. 154, 8–15, Japan, 2006.

25.  Takahashi, N., H. Shinagawa, D. Miyagi, Y. Doi, and K. Miyata, "Factors affecting eddy current losses of segmented Nd-Fe-B sintered magnets without insulation in large PM motors," *IEEE International Electric Machines and Drives Conference, IEMDC*, 24–29, 2009.

26.  Yamazaki, K., Y. Fukushima, and M. Sato, "Loss analysis of permanent magnet motors with concentrated windings — Variation of magnet eddy current loss due to stator and rotor shapes," *IEEE Transactions on Industry Applications*, Vol. 45, 1334–1342, 2009.

27.  Ferraris, L., P. Ferraris, A. Tenconi, and E. Poskovic, "Theoretic and experimental approach to the adoption of bonded magnets in fractional machines for automotive applications," *IEEE Transactions on Industrial Electronics*, Vol. 59, No. 5, 2309–2318, 2011.

28.  Jubb, G. and R. McCurrie, "Hysteresis and magnetic viscosity in a Nd-Fe-B permanent magnet," *IEEE Transactions on Magnetics*, Vol. 23, 1801–1805, 1987.

29.  Pfister, P. D., C. Koechli, M. Markovic, and Y. Perriard, "Analysis of hysteresis losses in synchronous permanent magnet motors," *2006 12th Biennial IEEE Conference on Electromagnetic Field Computation*, 144–144, 2006.

30.  Akatsu, K., K. Narita, Y. Sakashita, and T. Yamada, "Characteristics comparison between SPMSM and IPMSM under high flux density condition by both experimental and analysis results," *International Conference on Electrical Machines and Systems, 2008, ICEMS 2008*, 2848–2853, 2008.

31.  Ishak, D., Z. Q. Zhu, and D. Howe, "Eddy-current loss in the rotor magnets of permanent-magnet brushless machines having a fractional number of slots per pole," *IEEE Transactions on Magnetics*, Vol. 41, 2462–2469, 2005.

32.  Sergeant, P. and A. Van den Bossche, "Segmentation of magnets to reduce losses in permanent-magnet synchronous machines," *IEEE Transactions on Magnetics*, Vol. 44, 4409–4412, 2008.

33.  Yamazaki, K., M. Shina, Y. Kanou, M. Miwa, and J. Hagiwara, "Effect of eddy current loss reduction by segmentation of magnets in synchronous motors: Difference between interior and surface types," *IEEE Transactions on Magnetics*, Vol. 45, 4756–4759, 2009.

34. Pyrhonen, J., T. Jokien, and V. Hrabovcova, *Design of Rotating Electrical Machines*, John Wiely & Sons, Ltd., 2008.

35. Akita, H., Y. Nakahara, N. Miyake, and T. Oikawa, "A new core," *IEEE Industry Applications Magazine*, Vol. 11, 38–43, 2005.

36. Jack, A. G., B. C. Mecrow, P. G. Dickinson, D. Stephenson, J. S. Burdess, N. Fawcett, and J. T. Evans, "Permanent-magnet machines with powdered iron cores and prepressed windings," *IEEE Transactions on Industry Applications*, Vol. 36, 1077–1084, 2000.

37. Akita, H., Y. Nakahara, N. Miyake, and T. Oikawa, "New core structure and manufacturing method for high efficiency of permanent magnet motors," *Conference Record of the 2003 IEEE Industry Applications Conference, 38th IAS Annual Meeting*, Vol. 1, 367–372, 2003.

38. Emadi, A., *Energy-efficient Electric Motors*, 3rd Edition, Marcel Dekker, Inc., New York, 2005.

39. Bertotti, G., "General properties of power losses in soft ferromagnetic materials," *IEEE Transactions on Magnetics*, Vol. 24, 621–630, 1988.

40. Domeki, H., Y. Ishihara, C. Kaido, Y. Kawase, S. Kitamura, T. Shimomura, N. Takahashi, T. Yamada, and K. Yamazaki, "Investigation of benchmark model for estimating iron loss in rotating machine," *IEEE Transactions on Magnetics*, Vol. 40, 794–797, 2004.

41. Boglietti, A., A. Cavagnino, M. Lazzari, and M. Pastorelli, "Predicting iron losses in soft magnetic materials with arbitrary voltage supply: An engineering approach," *IEEE Transactions on Magnetics*, Vol. 39, 981–989, 2003.